ELSEVIER

NeuroImage

www.elsevier.com/locate/ynimg
NeuroImage 29 (2006) 1013 – 1022

Rapid Communication

Enhancing BOLD response in the auditory system by neurophysiologically tuned fMRI sequence

Erich Seifritz,[a,b,*] Francesco Di Salle,[c] Fabrizio Esposito,[d] Marcus Herdener,[a,b] John G. Neuhoff,[e] and Klaus Scheffler[f]

[a]*University Hospital of Clinical Psychiatry, University of Bern, 3000 Bern, Switzerland*
[b]*Department of Psychiatry, University of Basel, 4025 Basel, Switzerland*
[c]*Department of Neuroscience, University of Pisa, 56126 Pisa, Italy*
[d]*Department of Neurological Sciences, University of Naples Federico II, 80127 Naples, Italy*
[e]*Department of Psychology, The College of Wooster, Wooster, OH 44691, USA*
[f]*MR-Physics, Department of Medical Radiology, University of Basel, 4031 Basel, Switzerland*

Received 26 May 2005; revised 22 July 2005; accepted 23 August 2005
Available online 25 October 2005

Auditory neuroscience has not tapped fMRI's full potential because of acoustic scanner noise emitted by the gradient switches of conventional echoplanar fMRI sequences. The scanner noise is pulsed, and auditory cortex is particularly sensitive to pulsed sounds. Current fMRI approaches to avoid stimulus–noise interactions are temporally inefficient. Since the sustained BOLD response to pulsed sounds decreases with repetition rate and becomes minimal with unpulsed sounds, we developed an fMRI sequence emitting continuous rather than pulsed gradient sound by implementing a novel quasi-continuous gradient switch pattern. Compared to conventional fMRI, continuous-sound fMRI reduced auditory cortex BOLD baseline and increased BOLD amplitude with graded sound stimuli, short sound events, and sounds as complex as orchestra music with preserved temporal resolution. Response in subcortical auditory nuclei was enhanced, but not the response to light in visual cortex. Finally, tonotopic mapping using continuous-sound fMRI demonstrates that enhanced functional signal-to-noise in BOLD response translates into improved spatial separability of specific sound representations.

Introduction

The spatial and temporal resolution of BOLD fMRI catalyzed tremendous advance in brain research. However, auditory neuroscience has failed to take full advantage of fMRI's spatio-temporal information because of the acoustic noise produced by the data acquisition sequences. During echoplanar imaging and other fMRI sequences, acoustic noise is mainly produced by fast magnetic field gradient switches, which are necessary to generate spatial resolution. Slow gradient ramps (Jakob et al., 1998; Hennel et al., 1999; Loenneker et al., 2001) or experimental paradigm modifications with short scan times and long silent intervals between the scans (Scheffler et al., 1998; Hall et al., 1999) can avoid interaction between acoustic scanner noise- and stimulus-induced BOLD responses. Unfortunately, these techniques are temporally inefficient since functional data acquisition is typically limited to a few scans per minute. While fMRI with low temporal resolution primarily detects sustained neural activity associated with long-lasting stimuli, it typically disregards transient time-varying effects. If temporal resolution is required, specific techniques such as event-related averaged single trial paradigms must be employed, where the timing of functional image acquisition is shifted relative to the stimulus onset. This eventually allows the post hoc reconstruction of a composite signal profile as a function of timing relative to the stimulus (Ernst and Hennig, 1994; Robson et al., 1998; Belin et al., 1999). The inefficiency of such techniques to prepresent the temporal dynamics of BOLD responses to both short-lived and long-lasting sound properties at the same time is unfortunate considering the nonlinearity of the BOLD signal in the auditory system (Talavage and Edmister, 2004). The BOLD response is segregated into different temporal and spatial components in human (Seifritz et al., 2002) and animal auditory cortex (Recanzone, 2000), which possibly reflects different synaptic networks (Atzori et al., 2001). In addition, they differ with specific sound parameters and change dramatically across the human (Giraud et al., 2000; Griffiths et al., 2001; Harms and Melcher, 2002; Harms et al., 2005) and animal auditory pathway (Miller et al., 2001).

The acoustic noise generated by conventional echoplanar fMRI gradients is characterized by sound bursts occurring during each imaging slice. In fMRI data acquisitions without interruption between consecutive image slices within and between image volumes, this typically results in sound burst rates of 8 to 12 sound

* Corresponding author. University Hospital of Clinical Psychiatry, Bolligenstr. 111, 3000 Bern, Switzerland. Fax: +41 61 930 99 58.
E-mail address: seifritz@puk.unibe.ch (E. Seifritz).
Available online on ScienceDirect (www.sciencedirect.com).

1053-8119/$ - see front matter © 2005 Elsevier Inc. All rights reserved.
doi:10.1016/j.neuroimage.2005.08.029

events per second (depending on specific sequence parameters) that can excite auditory cortex during the image acquisition (Bandettini et al., 1998; Bilecen et al., 1998). Systematic studies evaluating the stimulus rate-dependence of the auditory cortex BOLD response have shown that repetition rates of 8–12 Hz produce BOLD signal amplitudes that are at least double as great compared to rates produced by stimulation rates of 30 Hz or higher; in addition, the sustained BOLD responses progressively decrease as repetition rates increase and single sound events perceptually fuse (Giraud et al., 2000; Tanaka et al., 2000; Harms and Melcher, 2002; Seifritz et al., 2003). Taking advantage of the repetition rate-dependent sensitivity decrease of BOLD response in the auditory cortex, we developed a novel fMRI sequence that produces a perceptually continuous rather than pulsed acoustic noise. Here, we describe the technical implementation of a novel continuous-sound fMRI sequence and present neurophysiological results obtained in a series of feasibility experiments geared towards the exploration whether this specific modification may increase the dynamic range of the BOLD response in the auditory system.

Materials and methods

Continuous-sound fMRI sequence design

Conventional fMRI (here, T_2^*-weighted single-shot gradient-recalled) is composed of slice-selective excitation followed by a read-out train, which consists of a rapidly switched, alternating read gradient and small phase-encoding gradient blips (Fig. 1A). The resulting gradient noise is thus characterized by a high-frequency component produced by the alternating read-out gradient plus a low-frequency component generated by the repetition of consecutive slices. Recording of conventional fMRI gradient noise and its power spectrum is shown in Figs. 1C and E. For continuous-sound fMRI, the read-out and phase-encoding gradients were divided into several short trains of echoes consisting of five read-out pairs (10 echoes) and 10 phase-encoding blips (Fig. 1B). Consecutive echo trains are separated by a period of 2.56 ms required for slice-selective excitation at the beginning of the echo train. Additional gradients required for slice selection, phase/read-dephasing, and -spoiling have been implemented with very low gradient amplitudes and long rise and fall times (2 ms) and were added to the continuously running read-out and phase-encoding blocks. A highly selective spectral fat saturation pulse has a duration of at least 5 to 10 ms which would produce an additional gap within the short trains of echoes. In order to preserve the continuos sound, these gaps have to be added between each short echo train. Because this would drastically increase volume repetition time (TR) and reduce imaging efficiency, no spectral fat sat was included in the continuous-sound fMRI sequence. Recording of continuous-sound fMRI gradient noise and its power spectrum is shown in Figs. 1D and F.

Imaging procedures

Healthy volunteers were recruited from an academic environment. All subjects had normal hearing and no history of major medical, neurological, or psychiatric disorders or of psychotropic

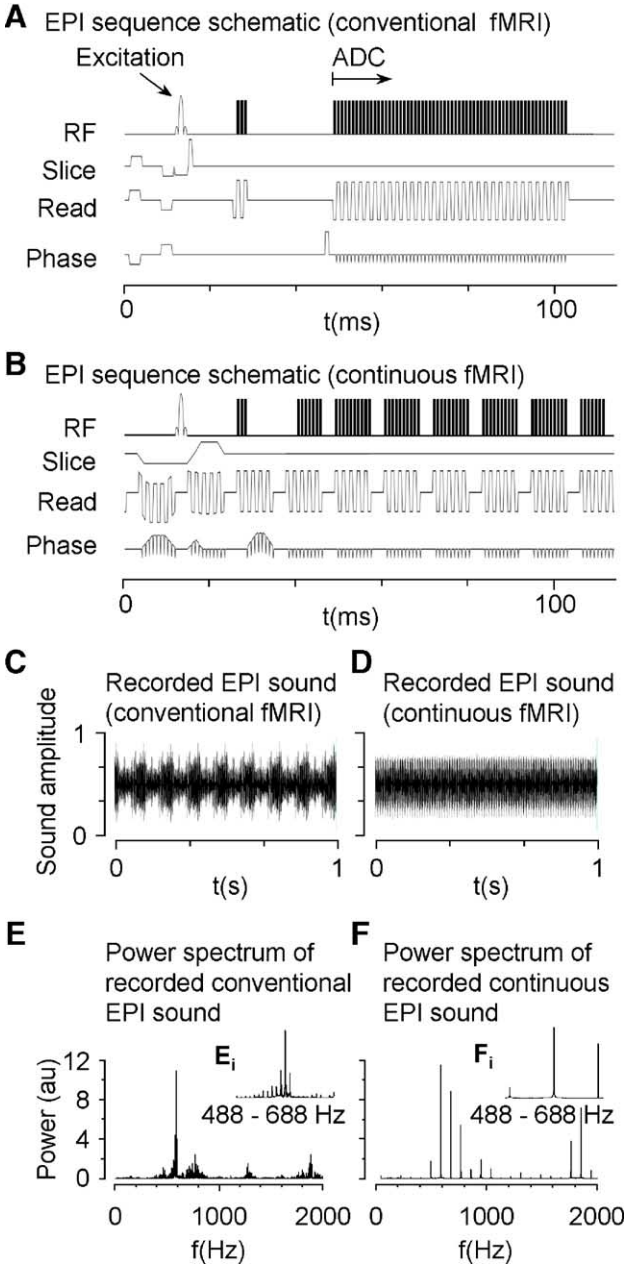

Fig. 1. Schematic of conventional (A) and continuous-sound (B) echo-planar fMRI showing radio-frequency pulse (RF), data sampling (ADC), and the three gradients. In terms of acoustic gradient sounds associated with the fMRI sequences, the noise pattern of conventional fMRI is determined mainly by the repetition of image slice acquisitions, which results in a pulsed sound with a repetition rate of 9.04 Hz (C). In contrast, the quasi-continuous read-out gradients and blips associated with continuous-sound fMRI produce a noise pattern with a repetition rate of 90.4 Hz (D). This repetition rate is faster than auditory fusion frequency and is perceived as continuous sound. The difference of sound pressure level time-courses is illustrated by the envelopes of the recorded fMRI gradient sounds shown in panels C and D. The corresponding power spectra of the recorded sound (C, D) show a main peak at 588 Hz for both fMRI variants (E, F). Since sampling length of the Fourier-transformed sound pattern was not an integer multiple of the low-frequency components, the 9.04 Hz (E) and 90.4 Hz (F) components appear as corresponding separation of multiple peaks around the 588 Hz center frequency. Inserts (E_i, F_i) show details of power spectra between 488 and 688 Hz and demonstrate a peak separation of 9.04 Hz and 90.4 Hz, respectively, reflecting the different sound envelopes (C, D).

medication. After having signed written informed consent, a total of 25 subjects (7 women, 18 men; age, 28.8 ± 6.2 years) were enrolled in one or more of fMRI experiments 1–7 (experiment 1, $N = 12$; experiment 2–7, $N = 6$). Images were acquired with 1.5 T (Siemens Sonata scanner with circularly polarized head coil; Siemens, Erlangen, Germany). Except for experiment 1, all experiments consisted of counterbalanced equal numbers of runs using continuous-sound and conventional fMRI with identical imaging parameters except for spectral fat saturation that was included in the conventional but not continuous-sound fMRI sequences. To avoid carry-over effects, the fMRI sequences were employed in pseudorandom and counterbalanced order across subjects. For the present comparison purposes, critical sequence parameters such as bandwidth, echo time (TE), echo spacing, TR, and spatial resolution were set identical for conventional and continuous-sound fMRI. Intrasession whole-brain T_1-weighted volumes (three-dimensional magnetization-prepared rapid acquisition gradient echo sequence by Mugler and Brookeman (1990) with a voxel size of 1 mm^3) were acquired. Functional slabs were positioned parallel to lateral sulcus to cover auditory and surrounding temporal cortex (experiments 1 and 3–7) or transversal to cover both auditory and visual cortex (experiment 2). Auditory stimuli were presented through headphones (Commander XG, Resonance Technology Inc., Northridge, CA, USA).

Experiment 1 (scanner noise-induced activity)

Stimuli: Tape-recorded (Brüel and Kjaer Sound and Vibration Measurement A/S, Naerum, Denmark) scanner noise associated with conventional and continuous-sound fMRI (for sound spectra and envelope see Fig. 1) was presented using a sparse image acquisition scheme as previously described (Bilecen et al., 1998). Stimulation paradigm: Auditory stimuli were presented alternatingly four times each in blocks of 76.6-s alternating with 76.6-s periods of no stimulation (silent baseline). Imaging parameters: FOV, 180^2 mm^2; matrix, 64^2 pixels (px); slice thickness, 4 mm; TE, 61 ms; flip angle, 90°; bandwidth, 1280 Hz/px; slice acquisition time, 110.6 ms; number of slices, 12; TR, 15.3 s; scan times, 1.33 s; silent interscan times, 14.0 s.

Experiment 2 (audio–visual comparison)

Stimuli: Pulsed sounds (sine tone, 1 kHz; repetition rate, 5 Hz; duty cycle, 50%; sound pressure level, 90 dB) and pulsed light (red light emitting 10 × 10 cm diode plate positioned at the bore of the magnet, approximately 75 cm in front of the eyes that were equipped with a mirror system; repetition rate, 5 Hz; duty cycle, 50%). Stimulation paradigm: Auditory and visual stimuli were presented alternatingly four times per run in blocks of 60-s alternating with 60-s periods of no stimulation (baseline, during which subjects heard only scanner noise and saw a dark diode plate). One run with conventional and one run with continuous-sound fMRI were carried out. Imaging parameters: FOV, 180^2 mm^2; matrix, 64^2 px; slice thickness, 5 mm; TE, 61 ms; flip angle, 90°; bandwidth, 1280 Hz/px; slice acquisition time, 110.6 ms; number of slices, 25; TR, 2.77 s.

Experiment 3 (sound contrast dependence)

Stimuli: Pulsed sounds (sine tone, 1 kHz; repetition rate, 5 Hz; duty cycle, 50%; sound pressure level, 90 dB) graded in pulse modulation depth yielding three contrasts (100%, 29.6%, 8.78%). Stimulation paradigm: Each sound contrast level was presented in pseudorandom order four times per run in blocks of 30-s alternating with 30-s periods of no stimulation (baseline, during which subjects heard only scanner noise). Contrast was defined according to Boynton et al. (1996) as follows: [high amplitude minus low amplitude] / [high amplitude + low amplitude]; note, that contrast thus covaries negatively with sound energy. One run with conventional and one run with continuous-sound fMRI were carried out. Imaging parameters: FOV, 180^2 mm^2; matrix, 64^2 px; slice thickness, 5 mm; TE, 61 ms; flip angle, 90°; bandwidth, 1280 Hz/px; slice acquisition time, 110.6 ms; number of slices, 16; TR, 1.77 s.

Experiment 4 (sound bandwidth dependence)

Stimuli: Pulsed bandpass white noise (center frequency, 1 kHz; repetition rate, 5 Hz; duty cycle, 50%; sound pressure level, 90 dB) graded in bandwidth (0.5–2 kHz [±1 octave], 0.25–4 kHz [±2 octaves], 0.125–8 kHz [±3 octaves]). Stimulation paradigm: Each sound bandwidth level was presented in pseudorandom order four times per run in blocks of 30-s alternating with 30-s periods of no stimulation (baseline, during which subjects heard only scanner noise). One run with conventional and one run with continuous-sound fMRI were carried out. Imaging parameters: FOV, 180^2 mm^2; matrix, 64^2 px; slice thickness, 5 mm; TE, 61 ms; flip angle, 90°; bandwidth, 1280 Hz/px; slice acquisition time, 110.6 ms; number of slices, 16; TR, 1.77 s.

Experiment 5 (sound spectral frequency dependence)

Stimuli: Pulsed sine tones (repetition rate, 5 Hz; duty cycle, 50%; sound pressure level, 90 dB) graded in spectral frequency yielding three pitches (125 Hz, 1 kHz, 8 kHz). Stimulation paradigm: Each spectral frequency level was presented in pseudorandom order four times per run in blocks of 30-s alternating with 30-s periods of no stimulation (baseline, during which subjects heard only scanner noise). One run with conventional and one run with continuous-sound fMRI were carried out. Imaging parameters: FOV, 180^2 mm^2; matrix, 128^2 px; slice thickness, 3 mm; TE, 64 ms; flip angle, 90°; bandwidth, 1260 Hz/px; slice acquisition time, 152 ms; number of slices, 15; TR, 2.28 s.

Experiment 6 (response to music)

Stimuli: Orchestra music (first 60 s of A. Vivaldi's Presto III in L'estate of Concerto no. 2 in G minor 'Le quattro stagioni' [RV315; English Chamber Orchestra, Church of St. John-at-Hackney London, violin and directed by N. Kennedy, 1986/9; EMI Records]; sound pressure level peak, 95 dB). Stimulation paradigm: One experimental run consisted of a baseline period of 50 s, during which subjects heard only scanner noise, and a period of 60 s during which music was presented. Three runs with conventional and three runs with continuous-sound fMRI were carried out. Imaging parameters: FOV, 180^2 mm^2; matrix, 64^2 px; slice thickness, 5 mm; TE, 61 ms; flip angle, 90°; bandwidth, 1280 Hz/px; slice acquisition time, 110.6 ms; number of slices, 16; TR, 1.77 s.

Experiment 7 (event-related response)

Stimuli: Short sound event (sine tone, 440 Hz; sound level, 80 dB; duration, 50 ms). Stimulation paradigm: Sound events had a stimulus onset asynchrony of 25–31 s, and were repeated six times per run. Two runs with conventional and two runs with continuous-sound fMRI were carried out. Imaging parameters: FOV, 180^2 mm^2; matrix, 64^2 px; slice thickness, 5 mm; TE, 61 ms; flip angle, 90°; bandwidth, 1280 Hz/px; slice acquisition time, 110.6 ms; number of slices, 16; TR, 1.77 s.

Image analyses

Functional image time-series were corrected for slice acquisition time, realigned with T_1-volumes, warped into standard space (Talairach and Tournoux, 1988), and corrected for head motion and low- and high-frequency fluctuations (linear detrending, 4 s gaussian kernel). In all but one experiment, functional data were resampled into 3-mm isotropic voxels and spatially smoothed with a 6-mm full-width at half-maximum gaussian kernel to account for interindividual spatial differences; in the tonotopy experiment 5, the results of which are presented on an individual level, functional data were resampled to 1 mm isometric voxels and not spatially smoothed to preserve spatial resolution (Fig. 7). These preprocessing steps were carried out using Brain Voyager (BrainInnovation, Maastricht, The Netherlands).

Stimulus-specific functions were convolved with single gamma functions to model hemodynamic response; time-series variance was estimated voxel-wise according to the general linear model (Friston et al., 1995), and appropriate fixed-effects linear contrasts were calculated. Reported P values are corrected for multiple voxel-wise comparisons (except for the subcortical activity in medial geniculate body shown in Fig. 5B, for which anatomo-functional a priori hypotheses implicitly protected against false positives).

Stimuli of experiments 3–5 were used to generate the general linear contrast shown in Figs. 5A and B. As a proof of concept, we examined the BOLD signal time-course of stimuli that did not contribute to the activity map in Figs. 5A and B and used the stimuli of experiments 6 and 7 to evaluate performance of continuous-sound compared to conventional fMRI. In a second level analysis, for the voxels that were statistically significant as main effects, spatial gradient maps – representing and color-coding the contribution of a given stimulus across a series of parametrically varied stimuli to the shared variance of the measured BOLD signal within an imaging voxel (Figs. 6 and 7) – were obtained using two descriptive approaches: (a) For group representations of bandwidth (*experiment 6*), the β values of each stimulus-specific predictor as estimated by the general linear model were considered. To avoid the generalized predominance of one bandwidth or frequency against the others, β values of each bandwidth and frequency were normalized across voxels in the region activated by the main effects of the stimuli at the group-level. A 'multiple relative contribution map' was finally obtained by assigning each voxel to a stimulus-parameter on the basis of the maximum normalized β and color-coding the parameters (Seifritz et al., 2002).

(b) For individual tonotopy, best-frequency-maps were computed – as previously suggested (Formisano et al., 2003) – in an attempt to exploit fully the increased spatial resolution of acquisition adopted for experiment 5. At each voxel, the averaged fractional signal change was estimated for the three frequencies relatively to the onset of the stimulation (event-related averaging). Then, voxels were assigned to the frequency for which the maximum fractional signal change was measured.

In the reported results, group-level statistical maps are superimposed on sections of Montreal Neurological Institute T_1-weighted brain template (www.bic.mni.mcgill.ca) and presented in radiological convention (right image side, left head side) as well as on an inflated cortical surface representation. The $x/y/z$-coordinates refer to standard space of Talairach and Tournoux (1988). Individual maps are superimposed on an inflated representation of the cortical surface obtained from segmentation and reconstruction of the individual whole brain high resolution T_1-weighted three-dimensional scans.

Results

The switched gradients of conventional fMRI (Fig. 1A) produce acoustic noise that is characterized approximately by two fundamental frequency components of 9.04 Hz and 588 Hz (Figs. 1C, E). In contrast, the quasi-continuous gradients (Fig. 1B) of continuous-sound fMRI produce a pattern of acoustic noise that is characterized by a high-frequency component of 588 Hz and a low-

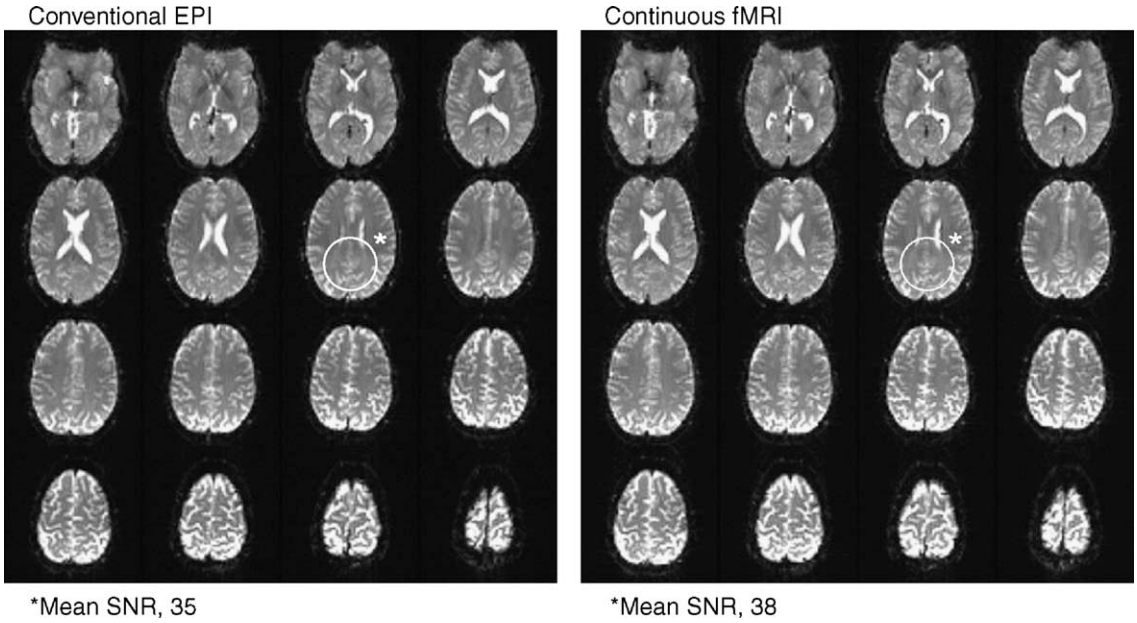

Fig. 2. Examples of human brain images acquired with conventional and continuous-sound fMRI. Both variants show comparable image warping and signal-to-noise ratio (SNR) and temporal signal stability.

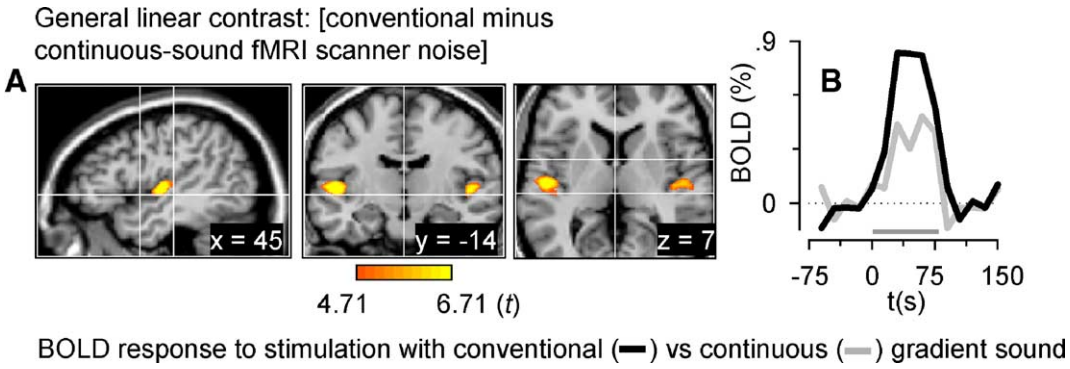

Fig. 3. Differential brain response to gradient noise emitted by conventional vs. continuous-sound fMRI as measured using (silent) sparse imaging in combination with headphone presentation of tape-recorded fMRI sound in 12 subjects (experiment 1). Sparse sampling was characterized by short scans (1.3 s) and long (14 s) silent intervals without scanning (functional slab covered auditory and surrounding temporal cortex). The activation map (A) represents the group general linear contrast between responses to stimulation with conventional vs. continuous-sound fMRI gradient noise ($P_{corrected} \leq 0.05$). (B) Signal time-course averaged across all subjects in auditory cortex shown in panel A (black line, BOLD response to stimulation with conventional fMRI sound; gray line, BOLD response to stimulation with continuous-sound fMRI gradient noise). This demonstrates that the baseline BOLD signal level associated with continuous-sound fMRI is lower than the baseline level during conventional fMRI.

frequency component of 90.4 Hz (Figs. 1D, F). The slowly switched slice-selecting gradients, in the current implementaion, are imperceptible by humans. In the power spectra, the different envelopes are represented by envelope-specific peak separations of 9.04 Hz (Fig. 1E_i) and 90.4 Hz (Fig. 1F_i). Psychoacoustically, the 9.04 Hz low-frequency component of conventional fMRI produces the percept of a pulsed interrupted sound pattern; in contrast, the 90.4 Hz low-frequency component of continuous-sound fMRI is perceived as a continuous uninterrupted sound. Sound pressure levels of conventional and continuous-sound fMRI sequences peaked at ~100 dB and were attenuated ~30 dB by the headphones. For the continuous-sound fMRI, sequence data are acquired with several short trains of echoes, which lead to a short echo spacing within the echo train (720 μs) and a longer echo spacing between echo trains (11060 μs). With such a nonlinear or stepwise increase of echo time along successive phase-encoding steps, signal fluctuations and image artifacts such as ghosting in regions with high susceptibility differences should be considered because of the following reason: for continuous-sound fMRI 64 echoes are splitted into 7 blocks of 10 echoes (first and last block only acquires 7 echoes). Therefore, the echo time of each single echo does not increase linearly as in conventional fMRI, but piecewise linearly with jumps of 2.56 ms within the blocks. This could lead to potential ghosting produced by jumps of the amplitude and phase of the echoes. In case of scanner instabilities or head movement, this not only would create image shifts but also changes of potential ghosting artifacts. However, in the brain, a very high field homogeneity can be achieved (20–30 Hz full-width at half-maximum), and phase errors along the echo train of continuous-sound fMRI are comparable to those of conventional fMRI. This was substantiated by comparison measurements, which revealed comparable signal-to-noise ratios (Fig. 2) and temporal signal stability (1.46% for conventional and 1.57% for continuos EPI) evaluated pixel-wise as standard deviation over mean signal

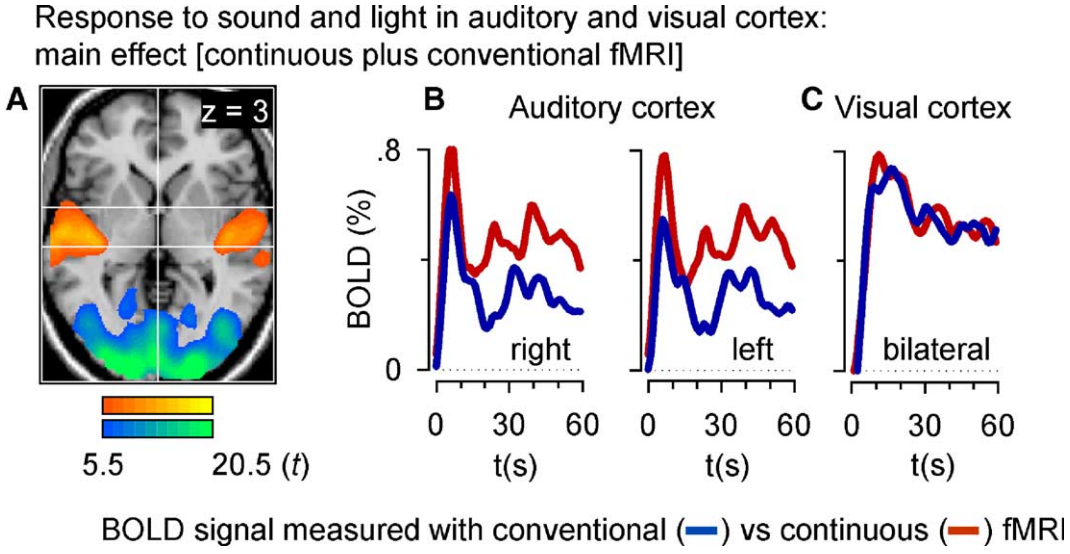

Fig. 4. (A) Main effects of response to pulsed sound and light measured with continuous-sound and conventional fMRI ($P_{corrected} \leq 0.001$). Corresponding BOLD signal time-course in auditory (B) and visual (C) cortex (red, measured with continuous-sound fMRI; blue, measured with conventional fMRI). Note, continuous-sound fMRI produced an enhanced BOLD signal only in the auditory but not in the visual system, demonstrating a domain-specific physiological effect.

along a time-series of 50 measurements (Weisskoff, 1996). In its current implementation, continuous-sound fMRI is ~15% slower than conventional fMRI; however, sequence optimization (e.g. shorter radio-frequency pulses and/or longer trains of echoes) may partially overcome this limitation. For example, longer echo trains, say 128, increase imaging efficiency since the ratio between echo block duration and block separation will be increased. However, our intention was to describe and present the principles of this new fMRI acquisition scheme rather than going into details of sequence design. In addition, the principle of quasi-continuous gradient-switching may be implemented in parallel, spiral, and other imaging sequence principles, and can take full advantage of any active and passive noise-attenuating measure.

As a proof of concept, we examined in experiment 1 the response to recorded fMRI sounds presented through headphones using sparse image sampling (Hall et al., 1999) in combination with conventional fMRI (with short scan and long silent interscan periods). The sustained BOLD signal level in auditory cortex (Fig. 3A) to played-back sound recordings of continuous-sound fMRI was approximately 50% of the signal level during presentation of recorded conventional fMRI sound (Fig. 3B). We therefore hypothesized that the decreased baseline – during which the subjects heard the scanner noise of continuous-sound fMRI but not an experimental stimulus – should increase the stimulated BOLD amplitude in the auditory but not the visual system. In experiment 2, we found enhanced response to pulsed sine tones in the auditory

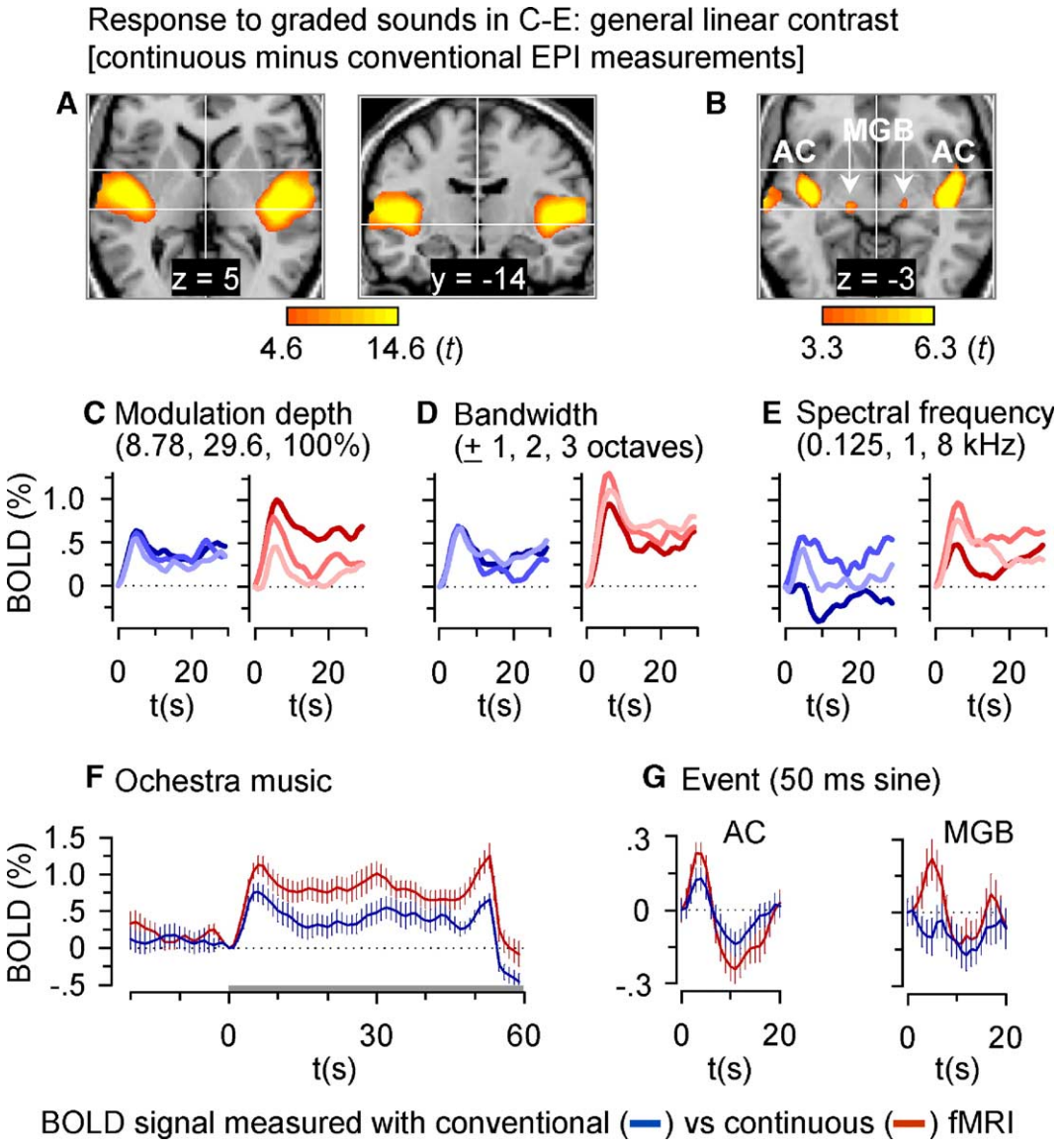

Fig. 5. General linear contrast between response to all graded sound stimuli shown in panels C–E measured with continuous-sound vs. conventional fMRI; (A) auditory cortex ([AC], $P_{corrected} \leq 0.05$) and (B) medial geniculate body ([MGB], $P_{uncorrected} \leq 0.001$). (C–E) The BOLD signal time-courses (red, measured with continuous-sound fMRI; blue, measured with conventional fMRI) are derived from auditory cortex (A), increasing color depths in plots represent increasing stimulus grades (experiments 3–5). (F) BOLD response in auditory cortex (A) to orchestra music (experiment 6; note, the gray bar represents the 60 s during which music was presented, the BOLD signal decrease at the end was not related to the end of stimulation but to a change in the musical properties); (G) BOLD response in auditory cortex (A) and medial geniculate body (B) to sine tone lasting 50 ms (experiment 7). Data in panels F and G are mean ± standard error.

cortex using continuous-sound compared to conventional fMRI (Figs. 4A, B); however, comparing continuous-sound and conventional fMRI, we did not find differential responses to light stimuli in the visual cortex (Figs. 4A, C).

In experiments 3–5, using graded sound stimuli, we found increased BOLD signal levels in auditory cortex (Fig. 5A) and in subcortical medial geniculate body (Fig. 5B). This was accompanied by a general gain in response modulation for stimulus grades (Figs. 5C–E) as well as for sound stimuli as complex as orchestra music (Fig. 5F) or as short as 50 ms (Fig. 5G, cortical and subcortical). For instance, consistent with the visual system (Boynton et al., 1996), sound contrast graded using pulse modulation depth, was closely related to the BOLD response; however, this association was stronger using fMRI with continuous-sound rather than conventional fMRI. Furthermore, we examined brain responses to stimuli, which have known topic representations in human and animal auditory cortex (Morel et al., 1993; Rauschecker et al., 1995; Wessinger et al., 1997; Talavage et al., 2000; Wessinger et al., 2001; Schönwiesner et al., 2002; Formisano et al., 2003). In experiment 4 (bandwidth dependence) and experiment 5 (spectral frequency dependence), we compared the results obtained with continuous-sound vs. conventional fMRI. The spatial representation of bandwidth dependence was characterized by a bandwidth-related centrifugal spatial gradient (Fig. 6). Narrow bandpass noise was preferred in the central areas corresponding to the core of the auditory cortex and broader bandpass noise was preferred in the surrounding areas corresponding to the belt of the auditory cortex. This pattern of response preference is consistent with previous human (Wessinger et al., 2001) and animal (Rauschecker et al., 1995) data. Continuous-sound fMRI (Fig. 6A), compared to conventional fMRI (Fig. 6B), yielded – at identical statistical thresholds – an extended and more detailed spatial representation of bandwidth in the auditory cortex. For spectral frequency dependence (Fig. 7), spatial representation was characterized by multiple best frequency areas reminiscent of previously described multiple frequency-dependent response regions (Talavage et al., 2000). In addition, the topography of these response regions was reminiscent of the presence of mirror-symmetric tonotopic maps in human (Formisano et al., 2003) and animal auditory cortex (Morel et al., 1993). The comparison of the subject-specific results obtained with continuous-sound (Fig. 7A) compared to conventional (Fig. 7B) fMRI – at the same statistical thresholds – demonstrates the translation of increased signal-to-noise within the BOLD signal response into improved spatial information.

Discussion

Current solutions to avoid interaction between acoustic scanner noise- and experimental stimulus-related brain activity such as sparse and averaged single trial image sampling, or silent gradient switching during fMRI are temporally highly inefficient or associated with low signal-to-noise ratio (Ernst and Hennig, 1994; Jakob et al., 1998; Robson et al., 1998; Scheffler et al., 1998; Belin et al., 1999; Hall et al., 1999; Hennel et al., 1999; Loenneker et al., 2001). Passive and active noise reduction measures, modified

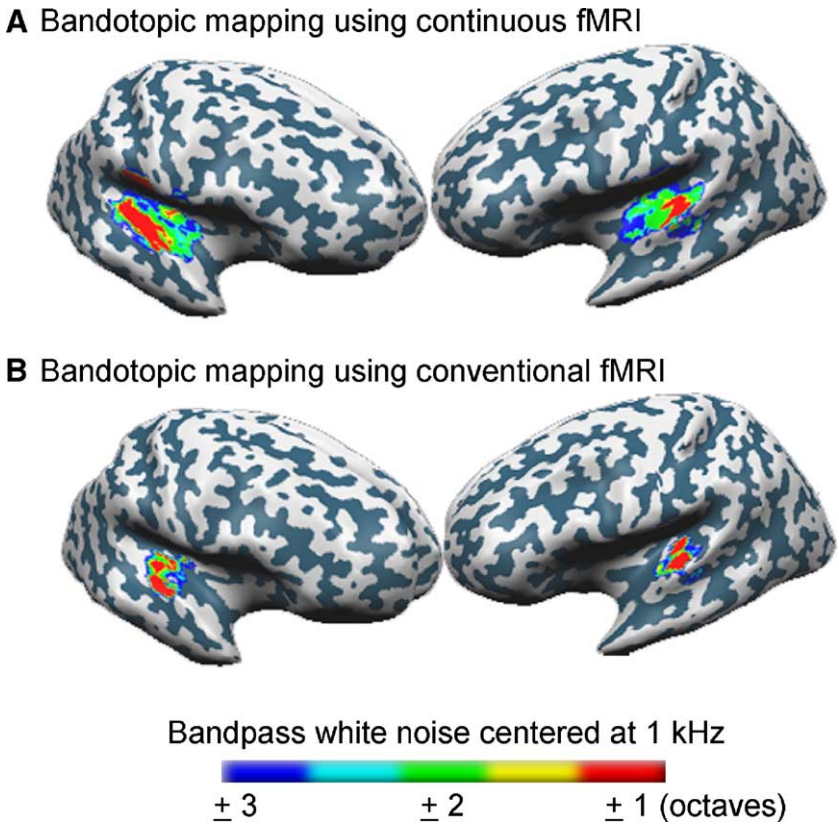

Fig. 6. Group representation of bandpass white noise with centrifugal activity pattern in the auditory cortex (experiment 4), as measured with continuous-sound (A) and conventional (B) fMRI. The central core regions of auditory cortex prefer narrow band noise, while belt regions prefer broad band noise. The BOLD signal time-courses are given in Fig. 5D.

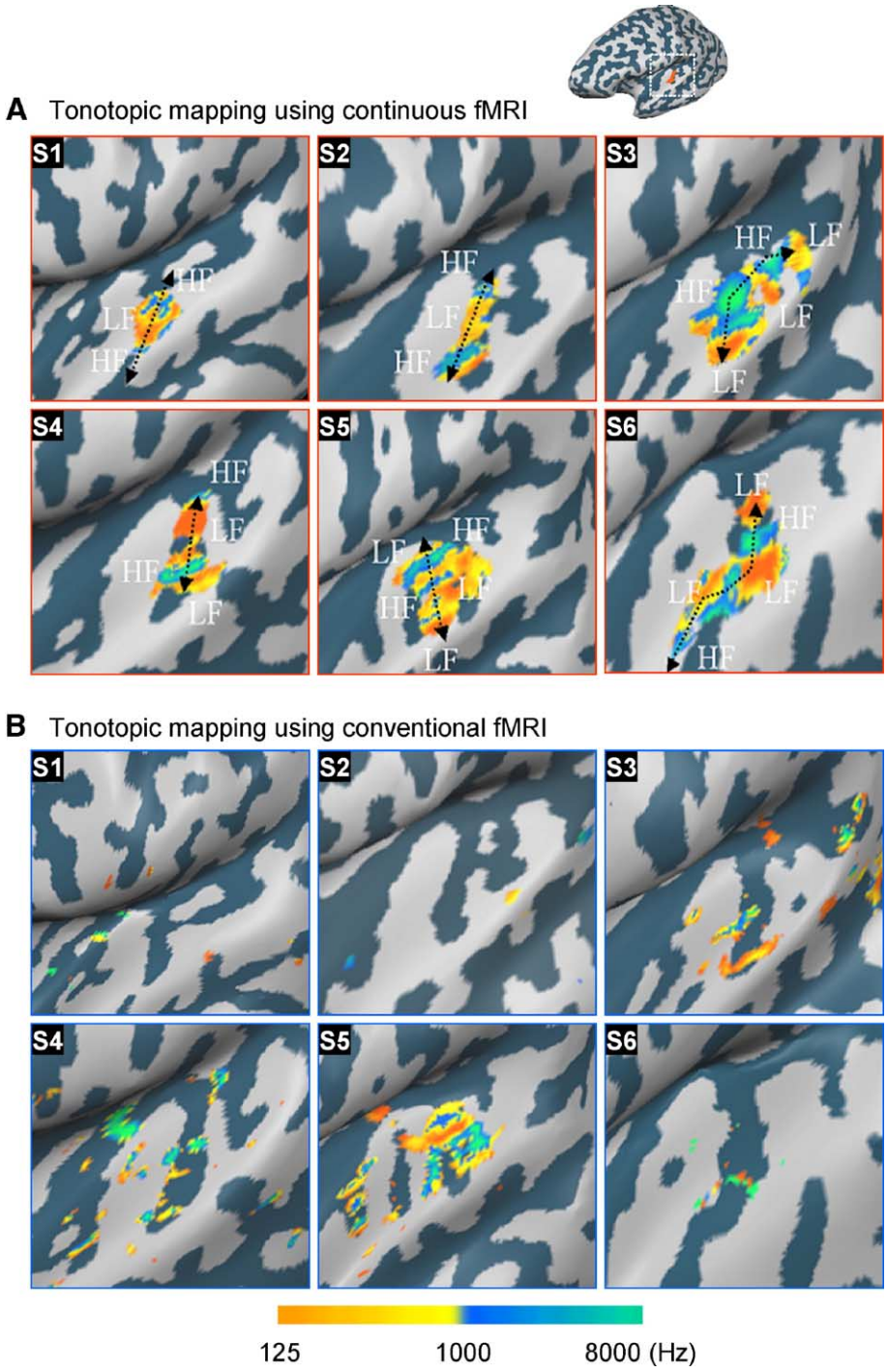

Fig. 7. Individual subject tonotopic mapping in six subjects (S1–6) obtained with continuous-sound and conventional fMRI. (A) Individual subjects' representation of three sound frequencies (experiment 5) suggesting the presence of tonotopic mirror-symmetric maps in the auditory cortex. (B) Same individual tonotopic maps obtained with conventional fMRI measurements at the same statistical threshold as in panel A. The BOLD signal time-courses are given in Fig. 5E.

gradients, and future scanner hardware improvement represent important leads to reduce perceivable scanner background noise (de Zwart et al., 2002; Tomasi and Ernst, 2003; Preston et al., 2004); such measures, however, can be implemented with the quasi-continuous gradient fMRI principle. The first experiment demonstrated that the basic assumption, that the unpulsed sound of fMRI with a quasi-continuous gradient switch pattern, as compared to the pulsed sound pattern of conventional fMRI, was associated with decreased 'resting-state' BOLD signal baseline.

The potential advantages of BOLD baseline reduction, which may lead to an enhanced dynamic reserve capacity of the BOLD signal response to experimental stimuli, are illustrated in a series of descriptive feasibility experiments: the continuous-sound fMRI detected tonotopic representations in auditory cortex, which were

not detected with conventional fMRI. Tonotopic mapping was obtained with preserved temporal resolution and yielded a pattern of activity, which was consistent with multiple response areas exhibiting specific frequency preference (Talavage et al., 2004). Most importantly, the spectral frequency-dependent topography was consistent with mirror-symmetric representations in animal (Morel et al., 1993) and human auditory cortex (Formisano et al., 2003). As such, the tonotopic mirror symmetry detected with continuous-sound fMRI was consistent with the results obtained previously using 7 T in combination with sparse sampling. We also found that continuous-sound compared to conventional fMRI detected bandwidth-dependent spatial representation in auditory cortex with greater sensitivity and specificity. The bandwidth-specific distribution was characterized by a centripetal spatial gradient with increasing preference for narrow-band noise in core and broad-band noise in belt areas of auditory cortex (Hackett et al., 2001). This spatial gradient is consistent with animal electrophysiological data (Rauschecker et al., 1995), and with human sparse acquisition fMRI data (Wessinger et al., 2001). In visual cortex, with the effects of flickering light, stimulus contrast is correlated with BOLD response amplitude (Boynton et al., 1996). For sound contrast modulation, here we found a similar relationship between sound contrast and BOLD response in auditory cortex. The observed relationship between sound contrast and BOLD response was strongly augmented with continuous-sound compared to conventional fMRI. This advantage will eventually be useful in detailing the relationship between neural activity and BOLD signal, which has been studied extensively in the visual system (Boynton et al., 1996; Davis et al., 1998; Hoge et al., 1999; Logothetis et al., 2001) but to a lesser extent in the auditory system. The increased sensitivity of continuous-sound fMRI in detecting and specifying BOLD responses to basic physical sound properties was particularly evidenced by the increased dynamic signal during the presentation of a stimulus as complex as orchestra music. In addition, continuous-sound fMRI yielded a greater BOLD response to short stimuli both in auditory cortex and medial geniculate body. So far, subcortical structures of the auditory pathway have only been studied using heart rate-triggered fMRI acquisition (Harms and Melcher, 2002; Krumbholz et al., 2005), a technique that is limited in terms of temporal resolution.

In conclusion, our findings demonstrate that fMRI with quasi-continuous gradient switches produce continuous rather than pulsed acoustic noise. Consistent with the repetition rate-dependent sensitivity decrease of BOLD response in the auditory system, the baseline BOLD signal during continuous-sound fMRI was lower than that during conventional fMRI, which contributes to an increase in the dynamic range of BOLD response to basic and complex acoustic stimuli. The technique preserves temporal resolution and the increased physiological signal-to-noise ratio can be translated into enhanced spatial functional contrast needed for example for tonotopic mapping. These properties of continuous-sound fMRI represent a clear advantage compared to conventional fMRI and an alternative to silent technique approaches to the exploration of the auditory system, specifically if temporal resolution is required. The current continuous-sound fMRI sequence should further be evaluated in terms of its impact on cognitive and psychoacoustic interferences. However, the present data suggest that it has the potential to open new perspectives on dynamic analysis of spatio-temporal representations of auditory information and in further functional parcellation of the human auditory cortex.

Acknowledgments

Supported by Swiss National Science Foundation (63-58040.99/PP00B-103012, PP00B-68783). Authors thank Kirstin Elsner, Thomas König, and Markus Klarhöfer for technical help. US-patent of continuous-sound fMRI sequence pending (ES, KS).

References

Atzori, M., Lei, S., Evans, D.I., Kanold, P.O., Phillips-Tansey, E., McIntyre, O., McBain, C.J., 2001. Differential synaptic processing separates stationary from transient inputs to the auditory cortex. Nat. Neurosci. 4, 1230–1237.

Bandettini, P.A., Jesmanowicz, A., Van Kylen, J., Birn, R.M., Hyde, J.S., 1998. Functional MRI of brain activation induced by scanner acoustic noise. Magn. Reson. Med. 39, 410–416.

Belin, P., Zatorre, R.J., Hoge, R., Evans, A.C., Pike, B., 1999. Event-related fMRI of the auditory cortex. NeuroImage 10, 417–429.

Bilecen, D., Radü, E.W., Scheffler, K., 1998. The MR tomograph as a sound generator: fMRI tool for the investigation of the auditory cortex. Magn. Reson. Med. 40, 934–937.

Boynton, G.M., Engel, S.A., Glover, G.H., Heeger, D.J., 1996. Linear systems analysis of functional magnetic resonance imaging in human V1. J. Neurosci. 16, 4207–4221.

Davis, T.L., Kwong, K.K., Weisskoff, R.M., Rosen, B.R., 1998. Calibrated functional MRI: mapping the dynamics of oxidative metabolism. Proc. Natl. Acad. Sci. U. S. A. 95, 1834–1839.

de Zwart, J.A., van Gelderen, P., Kellman, P., Duyn, J.H., 2002. Reduction of gradient acoustic noise in MRI using SENSE-EPI. NeuroImage 16, 1151–1155.

Ernst, T., Hennig, J., 1994. Observation of a fast response in functional MR. Magn. Reson. Med. 32, 146–149.

Formisano, E., Kim, D.S., Di Salle, F., van de Moortele, P.F., Ugurbil, K., Goebel, R., 2003. Mirror-symmetric tonotopic maps in human primary auditory cortex. Neuron 40, 859–869.

Friston, K., Holmes, A., Worsley, K., Poline, J., Frith, C., Frackowiak, R., 1995. Statistical parametric maps in functional imaging—A general linear approach. Hum. Brain Mapp. 2, 189–210.

Giraud, A.L., Lorenzi, C., Ashburner, J., Wable, J., Johnsrude, I., Frackowiak, R., Kleinschmidt, A., 2000. Representation of the temporal envelope of sounds in the human brain. J. Neurophysiol. 84, 1588–1598.

Griffiths, T.D., Uppenkamp, S., Johnsrude, I., Josephs, O., Patterson, R.D., 2001. Encoding of the temporal regularity of sound in the human brainstem. Nat. Neurosci. 4, 633–637.

Hackett, T.A., Preuss, T.M., Kaas, J.H., 2001. Architectonic identification of the core region in auditory cortex of macaques, chimpanzees, and humans. J. Comp. Neurol. 441, 197–222.

Hall, D.A., Haggard, M.P., Akeroyd, M.A., Palmer, A.R., Summerfield, A.Q., Elliott, M.R., Gurney, E.M., Bowtell, R.W., 1999. "Sparse" temporal sampling in auditory fMRI. Hum. Brain Mapp. 7, 213–223.

Harms, M.P., Melcher, J.R., 2002. Sound repetition rate in the human auditory pathway: representations in the waveshape and amplitude of fMRI activation. J. Neurophysiol. 88, 1433–1450.

Harms, M.P., Guinan Jr., J.J., Sigalovsky, I.S., Melcher, J.R., 2005. Short-term sound temporal envelope characteristics determine multisecond time patterns of activity in human auditory cortex as shown by fMRI. J. Neurophysiol. 93, 210–222.

Hennel, F., Girard, F., Loenneker, T., 1999. "Silent" MRI with soft gradient pulses. Magn. Reson. Med. 42, 6–10.

Hoge, R.D., Atkinson, J., Gill, B., Crelier, G.R., Marrett, S., Pike, G.B., 1999. Linear coupling between cerebral blood flow and oxygen consumption in activated human cortex. Proc. Natl. Acad. Sci. U. S. A. 96, 9403–9408.

Jakob, P.M., Schlaug, G., Griswold, M., Lovblad, K.O., Thomas, R., Ives, J.R., Matheson, J.K., Edelman, R.R., 1998. Functional burst imaging. Magn. Reson. Med. 40, 614–621.

Krumbholz, K., Schönwiesner, M., Rubsamen, R., Zilles, K., Fink, G.R., von Cramon, D.Y., 2005. Hierarchical processing of sound location and motion in the human brainstem and planum temporale. Eur. J. Neurosci. 21, 230–238.

Loenneker, T., Hennel, F., Ludwig, U., Hennig, J., 2001. Silent BOLD imaging. MAGMA 13, 76–81.

Logothetis, N.K., Pauls, J., Augath, M., Trinath, T., Oeltermann, A., 2001. Neurophysiological investigation of the basis of the fMRI signal. Nature 412, 150–157.

Miller, L.M., Escabi, M.A., Read, H.L., Schreiner, C.E., 2001. Functional convergence of response properties in the auditory thalamocortical system. Neuron 32, 151–160.

Morel, A., Garraghty, P.E., Kaas, J.H., 1993. Tonotopic organization, architectonic fields, and connections of auditory cortex in macaque monkeys. J. Comp. Neurol. 335, 437–459.

Mugler III, J.P., Brookeman, J.R., 1990. Three-dimensional magnetization-prepared rapid gradient-echo imaging (3D MP RAGE). Magn. Reson. Med. 15, 152–157.

Preston, A.R., Thomason, M.E., Ochsner, K.N., Cooper, J.C., Glover, G.H., 2004. Comparison of spiral-in/out and spiral-out BOLD fMRI at 1.5 and 3 T. NeuroImage 21, 291–301.

Rauschecker, J.P., Tian, B., Hauser, M., 1995. Processing of complex sounds in the macaque nonprimary auditory cortex. Science 268, 111–114.

Recanzone, G.H., 2000. Response profiles of auditory cortical neurons to tones and noise in behaving macaque monkeys. Hear. Res. 150, 104–118.

Robson, M.D., Dorosz, J.L., Gore, J.C., 1998. Measurements of the temporal fMRI response of the human auditory cortex to trains of tones. NeuroImage 7, 185–198.

Scheffler, K., Bilecen, D., Schmid, N., Tschopp, K., Seelig, J., 1998. Auditory cortical responses in hearing subjects and unilateral deaf patients as detected by functional magnetic resonance imaging. Cereb. Cortex 8, 156–163.

Schönwiesner, M., von Cramon, D.Y., Rubsamen, R., 2002. Is it tonotopy after all? NeuroImage 17, 1144–1161.

Seifritz, E., Esposito, F., Hennel, F., Mustovic, H., Neuhoff, J.G., Bilecen, D., Tedeschi, G., Scheffler, K., Di Salle, F., 2002. Spatiotemporal pattern of neural processing in the human auditory cortex. Science 297, 1706–1708.

Seifritz, E., Salle, F.D., Esposito, F., Bilecen, D., Neuhoff, J.G., Scheffler, K., 2003. Sustained blood oxygenation and volume response to repetition rate-modulated sound in human auditory cortex. NeuroImage 20, 1365–1370.

Talairach, P., Tournoux, J., 1988. A Stereotactic Coplanar Atlas of the Human Brain. Thieme, Stuttgart.

Talavage, T.M., Edmister, W.B., 2004. Nonlinearity of FMRI responses in human auditory cortex. Hum. Brain Mapp. 22, 216–228.

Talavage, T.M., Ledden, P.J., Benson, R.R., Rosen, B.R., Melcher, J.R., 2000. Frequency-dependent responses exhibited by multiple regions in human auditory cortex. Hear. Res. 150, 225–244.

Talavage, T.M., Sereno, M.I., Melcher, J.R., Ledden, P.J., Rosen, B.R., Dale, A.M., 2004. Tonotopic organization in human auditory cortex revealed by progressions of frequency sensitivity. J. Neurophysiol. 91, 1282–1296.

Tanaka, H., Fujita, N., Watanabe, Y., Hirabuki, N., Takanashi, M., Oshiro, Y., Nakamura, H., 2000. Effects of stimulus rate on the auditory cortex using fMRI with 'sparse' temporal sampling. NeuroReport 11, 2045–2049.

Tomasi, D.G., Ernst, T., 2003. Echo planar imaging at 4 Tesla with minimum acoustic noise. J. Magn. Reson. Imaging 18, 128–130.

Weisskoff, R.M., 1996. Simple measurement of scanner stability for functional NMR imaging of activation in the brain. Magn. Reson. Med. 36, 643–645.

Wessinger, C.M., Buonocore, M.H., Kussmaul, C.L., Mangun, G.R., 1997. Tonotopy in human auditory cortex examined with functional magnetic resonance imaging. Hum. Brain Mapp. 5, 18–25.

Wessinger, C.M., VanMeter, J., Tian, B., Van Lare, J., Pekar, J., Rauschecker, J.P., 2001. Hierarchical organization of the human auditory cortex revealed by functional magnetic resonance imaging. J. Cogn. Neurosci. 13, 1–7.